Journal of Materials Chemistry C

ROYAL SOCIETY OF CHEMISTRY

PAPER

View Article Online
View Journal | View Issue

Cite this: *J. Mater. Chem. C*, 2024, **12**, 2084

Tailoring the properties of semi-aromatic copolyimides through structural manipulation towards energy-storage applications†

Irina Butnaru, * Adriana-Petronela Chiriac, Mihai Asandulesa, Codrin Tugui, Iuliana Stoica and Mariana-Dana Damaceanu

Received 15th November 2023,
Accepted 25th December 2023

DOI: 10.1039/d3tc04209j

rsc.li/materials-c

To enlarge the library of dielectric materials suitable for energy storage applications, three series of semi-aromatic copolyimides were developed by structural manipulation which enabled properties to be modulated. Various polar units such as nitrile, carbonyl, polyethylene and polypropylene oxide were integrated into the same polymer chains in different ratios to attain desirable characteristics. By WAXD, AFM, DSC and TGA the amorphous nature and high thermostability of copolyimide films were demonstrated, with no crystallization or phase separation, being shaped by the amount and nature of the soft segment. According to the mechanical and dielectric evaluation, a slight variation of copolymer composition tailored these properties in large limits, changing the material from a rigid to a flexible or even stretchable one, from a common material to one with self-sticky ability, from a low-*k* to a high-*k* material, all these being possible by an efficient chemical strategy. The electrical breakdown strength and energy storage performance were also governed by the chemistry design, the best value (326 kV mm^{-1} and 1.36 J cm^{-3}, respectively) being obtained for copolyimide containing the highest aromaticity and the lowest aliphatic chain length. Thus, the ability of the constitutive hard and soft segments to interpenetrate and to arrange in the polymer network led to films with variable and distinct properties suitable for use as flexible/stretchable dielectric materials or energy storage capacitors.

Introduction

Due to the fast development of the global economy and the rising population, the search for efficient, clean and renewable energy has evolved as a focal point of interest worldwide. In the accelerating landscape of energy storage technology, researchers and engineers are continuously seeking materials that can enhance the performance, durability, and safety of energy storage devices.[1–3]

Capacitors are essential components in electronic products and fit in a wide range of industrial applications, being a vital part of energy storage devices. Several dielectric materials have been developed so far for high-temperature capacitor applications, including ceramics and dielectric polymers, each of them having its own limitations.[4] The main drawback of ceramic film capacitors is their low breakdown strength and flexibility, and despite the advantages of high dielectric permittivity and thermal stability, their application in the energy storage field is limited.[5] Dielectric capacitors include the dielectric material as a key component, which governs the overall performance of the capacitors due to their properties. It is well-known that a dielectric capacitor stores and releases energy by a local dipole cyclization mechanism, which assures rapid charge and discharge rates, thus enabling a higher power density.[4] On the other hand, polymer-based dielectrics have been used in the fabrication of energy storage capacitors by virtue of their inherent flexibility, facile processing, high breakdown strength, low dielectric loss and ease of customizing continuous large area films with micron thickness.[6–10] Still, an existing issue remains which is represented by the insufficient thermal stability of the current polymeric materials developed for such applications. Moreover, when the requirements of high energy density corroborated with efficient thermal conductivity are added, the library of polymer-based dielectric materials is greatly narrowed.

Among the state-of-the-art polymer dielectrics suitable for high temperature film capacitors, polycarbonate (T_g = 150 °C for 6 μm film), poly(ether-ether-ketone) (T_g = 150 °C for 12 μm film), fluorene polyester (T_g = 330 °C for 6 μm film), polyetherimide (T_g = 217 °C for 12 μm film) and Kapton polyimide (T_g = 360 °C for 12 μm film) were taken into consideration since

"Petru Poni" Institute of Macromolecular Chemistry, Aleea Gr. Ghica Voda 41A, Iasi, 700487, Romania. E-mail: butnaru.irina@icmpp.ro

† Electronic supplementary information (ESI) available. See DOI: https://doi.org/10.1039/d3tc04209j

they are stable at the processing operating temperatures.[11] In addition, the influence of dielectric breakdown strength and dielectric constant on the value of energy density makes high performance polymers suitable materials for energy storage applications since these parameters determine the reliability and durability of dielectric polymers.[12–14]

The high degree of aromaticity and the presence of thermally stable rigid imide rings make polyimides able to withstand extreme temperatures without significant degradation, ensuring long-term reliability. The attractive mechanical properties, including high tensile strength and excellent dimensional stability, are crucial aspects for maintaining the structural integrity in energy storage components, particularly in demanding environments. The excellent insulating properties of polyimides are vital for minimizing energy losses due to parasitic capacitance in capacitive energy storage systems. Moreover, chemical resistance to a wide range of solvents is important for protecting energy storage components from corrosive environments or interactions with electrolytes. A particular aspect of polyimides is their ability to be tailored so as to possess various degrees of flexibility and processability, depending on the macromolecular structural design.[15–17] This versatility allows for customization to suit different energy storage device designs and configurations. One strategy was to incorporate various fillers like ceramic nanofillers Al_2O_3,[18] HfO_2 and TiO_2,[19] $CaCu_3Ti_4O_{12}$,[20] boron nitride nanosheets and $BaTiO_3$,[21] or graphene-based conductive nanofillers[22] into the polyimide matrix in order to improve the dielectric properties. Yet, these fillers cause a series of issues including incompatibility or agglomeration of the two constituent components of the composite materials which determined a decrease in insulating properties and difficulty in synthesis.[23] In the frame of these aspects, functional polyimides designed by manipulating the macromolecular architecture in term of short-range chain distance and geometric alignment enabled the optimization and improvement of properties in order to obtain increased values for electrical features.[7] Thus, to our knowledge, the highest value for energy density was obtained for the polyimide based on an aliphatic diamine (Jeffamine HK511) and a carbonyl-containing aromatic dianhydride (benzophenone tetracarboxylic dianhydride, BTDA), which had a dielectric constant of 7.8 and a maximum energy density of 15.77 J cm^{-3} but with a lower heat resistance in terms of glass transition temperature (T_g = 78 °C).[24] The 50–50% polyimide blend of Matrimid 5218 and Ultem 1000 recorded a relatively low dielectric constant of 3, a breakdown strength of 1000 MV m^{-1} at room temperature, and an energy density of 8 J cm^{-3}.[7] Incorporation of two polar pendant nitrile units in the main chain of polyimide derived from BTDA and a 2CN-based aromatic diamine enabled a dielectric constant of 4.8, a low dielectric loss of 0.00157 at 1 kHz and 25 °C, and a maximum energy density of 1.02 J cm^{-3}.[25] The introduction of polar sulfonyl groups in the polyimide based on 4,4-oxydiphthalic anhydride and an aromatic diamine with *para–para* linkage led to a dielectric constant of 5.98, a low dielectric loss of 0.00373 at 1 kHz, a discharge energy density of 7.60 J cm^{-3} and charge–discharge efficiency of 91.3% at 500 MV m^{-1}.[26] The polyimide derived from BTDA and a bipyridine-containing diamine determined the rise of the dielectric constant to 7.2, a dielectric loss of 0.038 and an energy storage density of 2.77 J cm^{-3}.[27] Polyimide based on BTDA, Jeffamine HK511 and hexane-1,6-diamine enabled a dielectric constant of 4.77, a dielectric loss <0.01, and an energy density of 12 J cm^{-3}.[28] An overall view of the performance of some commercially available polyimides and of several developed polyimide films is presented in Table S1 (ESI†).

Considering the literature data, it was obvious that a combination of various polar groups grafted on an imide-aromatic skeleton may enable the development of suitable materials for efficient energy storage applications. Our previous report on copolyimides based on BTDA, Jeffamine with a molar mass of 2000 Da and various nitrile-based aromatic diamines revealed the substantial influence of the position of polar nitrile groups on the overall properties of the free-standing films made therefrom.[29] Following a similar trend, the present work aims to evidence the influence of the nature (molar mass) of the aliphatic soft segment and its variable loading amount onto the physico-chemical behavior of the copolyimides, focusing on mechanical and dielectric characteristics. Thus, by varying the nature and quantity of the Jeffamine component, 3 series of copolymers with increasing amounts of the soft component were synthesized and the structure–property correlations were established. Due to the ability of the soft and hard constitutive components of the copolyimides to interpenetrate and to arrange in the polymer network, films with variable, distinct and tailorable properties were obtained which were successfully explored as dielectrics and thin film capacitors for energy storage.

Experimental

Starting materials

Jeffamine® ED-2003 (*O*,*O*′-bis(2-aminopropyl)polypropylene glycol-*block*-polyethylene glycol-*block*-polypropylene glycol, J-2000), Jeffamine® ED-900 (*O*,*O*′-bis(2-aminopropyl)polypropylene glycol-*block*-polyethylene glycol-*block*-polypropylene glycol, J-900), Jeffamine® ED-600 (*O*,*O*′-bis(2-aminopropyl)polypropylene glycol-*block*-polyethylene glycol-*block*-polypropylene glycol, J-600), *N*-methyl pyrrolidone (NMP anhydrous, 99.5%), *N*,*N*′-dimethylacetamide (DMAc, HPLC grade), dimethyl sulfoxide (DMSO anhydrous, ≥99.9%), tetrahydrofuran (THF, anhydrous, ≥99.9%), chloroform (anhydrous, 99%) and ethanol (analytical standard) were purchased from Sigma-Aldrich and used without purification. 3,3′,4,4′-Benzophenonetetracarboxylic dianhydride (BTDA, ≥97%) was acquired from Sigma-Aldrich and purified by standard procedures.

Aromatic diamine 2,6-bis(3-amino-phenoxy)-benzonitrile was synthesized according to a published procedure.[30]

Synthesis of copolyimides

Three series of copolyimides with a molar ratio of CN-functionalized aromatic diamine: Jeffamine-based aliphatic diamine of 0.7 : 0.3 (**coPI1–coPI3**), 0.6 : 0.4 (**coPI4–coPI6**) and 0.5 : 0.5

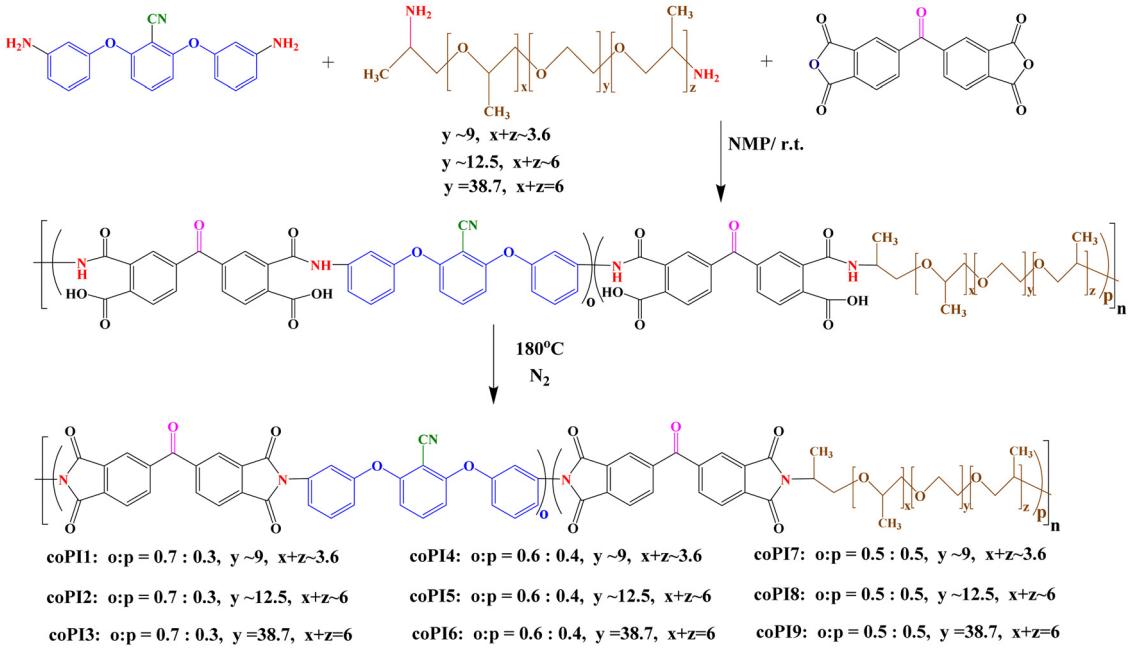

Scheme 1 Synthesis of copolyimides **coPI1–coPI9**.

(**coPI7–coPI9**) were obtained by classical two-step solution polycondensation reactions in NMP, at a concentration of 20% (Scheme 1).

In order to perform the synthesis, the aromatic dianhydride was used in an equimolecular quantity with respect to the mixture of the two diamines (aromatic and aliphatic). Therefore, three different molar ratios between CN-functionalized aromatic diamines and aliphatic diamines (0.7 : 0.3, 0.6 : 0.4 and 0.5 : 0.5, respectively) and three aliphatic diamines with various molecular weights of 600, 900 and 2000 Da were used in the synthesis of copolyimides.

The synthesis of **coPI4** with a molar ratio of CN-functionalized aromatic diamine: Jeffamine-based aliphatic diamine (J-600) = 0.6 : 0.4 is further given as an illustrative example. In a 100 mL three-necked round-bottom flask, fitted with a nitrogen inlet and outlet, 0.5 g (1.57 mmol) of 2,6-bis(3-aminophenoxy)-benzonitrile, 0.6 mL (1.05 mmol) of Jeffamine® ED-900 (J-900) and 4 mL of NMP were added. The diamine mixture was stirred under a nitrogen stream for 30 minutes until complete dissolution occurred. After that, 0.846 g (2.62 mmol) of BTDA and 3.9 mL of NMP were introduced in the flask, forming a yellow clear solution of copoly(amidic acid), which was stirred at room temperature for 16 h. In the second reaction stage, the intermediary copoly(amidic acid) solution was heated at 180 °C for 6 h. In order to remove the water evolved during the imidization process resulting from the dehydrating process, a strong stream of nitrogen was flowed through the system. It was noticed a variation of the solution color from light-yellow to dark brown with the evolution of the cyclodehydration process of the intermediary copoly(amidic acid). The final copolyimide viscous solution was precipitated in methanol, filtered, and washed several times with methanol. Solid light brown fibers were obtained, which were dried at 80 °C for 6 h.

Free-standing films

The copolyimide films were obtained from **coPI1–coPI9** as free-standing materials by dissolving a certain amount of copolymer powder in THF as a solvent. Thus, copolyimide solutions with a content of 10% in solids were prepared and filtered through a 45 μm filter syringe, then casted onto clean glass plates and placed in an ambient atmosphere for 24 h to slowly evaporate THF. The flexible films obtained after detaching from the support, with thickness values in the range of 35–55 μm, were used for various measurements.

Measurements

The ^{1}H NMR spectra were recorded on a Bruker Avance III 400 spectrometer operating at 400.1 MHz. ^{1}H chemical shifts are expressed in δ units (ppm) with respect to the residual peak of the solvent (^{1}H: $CDCl_3$ 7.26 ppm).

The Fourier-transform infrared spectroscopy (FTIR) measurements were performed on an FT-IR Bruker Vertex 70 spectrophotometer. The samples were in the form of film strips and analyzed in the ATR mode.

Gel permeation chromatography (GPC) was used to estimate the average molecular weights by using a ParSEC Chromatography Ver. 5.67 Brookhaven Instruments Corp. apparatus provided with refraction and UV detectors and PL Mixed C Column. The measurements were performed in DMF as a solvent with copolymer solutions prepared at a concentration of 0.5% after filtration. Standards of polystyrene with a known molecular weight were used for calibration.

Thermogravimetric analysis (TGA) was performed on a NETZSCH TG209 F1 Iris instrument, by using copolymer film samples of about 8 mg each. The sample was heated from 25 to 700 °C at a heating rate of 10 °C min^{-1}. The measurements were recorded under a nitrogen gas flow of 50 mL min^{-1}.

The glass transition temperature (T_g) of copolyimides was determined on the basis of differential scanning calorimetry (DSC) experiments. The analysis was carried out using a Mettler T28E calorimeter by heating the film samples under a nitrogen atmosphere from 25 to 300 °C, at a heating rate of 20 °C min^{-1}. After following heating–cooling–heating scans, T_g was estimated from the DSC diagram obtained in the second heating cycle.

Wide X-ray diffraction (WAXD) patterns were recorded on a Bruker AD8 Avance diffractometer, by using Ni-filtered Cu-Kα radiation (λ = 0.1541 nm) at 36 kV and 30 mA. All diffractograms were obtained on copolyimide films at room temperature, in the range of 2–40 (2θ degrees) and reported as obtained. The *d*-spacing values were calculated from the diffraction peak maximum, by using the Bragg equation:

$$d = \lambda/2 \sin\theta$$

where λ represents the wavelength of the radiation and 2θ is the angle corresponding to the maximum intensity of the amorphous halo exhibited by the polymer.

The morphology of the free-standing copolyimide films was investigated by atomic force microscopy (AFM) on a Scanning Probe Microscopy Solver PRO-M, NT-MDT equipment made in Russia, in semi-contact mode and semi-contact topography technique.

Mechanical measurements were conducted using an Instron 3365 machine equipped with a 500 N load cell. Tensile and cyclic tests were performed on dumbbell-shaped specimens that were extended at a rate of 10 mm min^{-1}. The deformation protocol employed to generate the cyclic curves and the calculation method of permanent deformation, recovery strain, tensile strength and toughness were detailed in the previous report.[29]

The dielectric spectroscopy investigations were carried out with the Broadband Dielectric Spectrometer (Novocontrol Technologies, Germany). The dielectric spectra were recorded at temperatures between −150 °C and 200 °C, by sweeping the frequency between 1 Hz and 1 MHz at every 5 °C. For these measurements, the free-standing films were sandwiched between two gold coated plate electrodes, which were placed in a dry nitrogen atmosphere.

Dielectric strength was evaluated by applying a stepwise increase in voltage, from 0 V to 20 KV, to each film sample at a rate of 100 V s^{-1}, until breakdown occurred. The Weibull analysis was carried out based on the results of 10 breakdown tests for each sample, following the procedure previously reported.[29]

The energy density (Ue) value of the copolyimide film materials was calculated based on the following equation:

$$\mathrm{Ue} = \frac{1}{2}\varepsilon'\varepsilon_o {E_{BD}}^2$$

where ε' is the dielectric permittivity of the material, ε_o represents the permittivity of the free space (8.85×10^{-12} F m^{-1}) and E_{BD} is the electrical breakdown strength.

Results and discussion

In an attempt to obtain multifunctional polyimide-based materials with variable physico-chemical properties by starting always from the same constituent monomers, the synergistic combination between a soft semi-aromatic segment and a hard aromatic fragment was approached towards three series of copolyimides. First, the polyimide chains were modified with polar nitrile groups, which in conjunction with carbonyl, polyethylene and polypropylene oxide units are expected to provide appealing physical and chemical features with respect to classical or even semi-aromatic polyimides. Then, a systematic variation of the molar ratio between the soft and hard segments was employed along with Jeffamines of distinct molecular weights, targeting to obtain free-standing films of variable flexibility or stretchability, and tuned characteristics relevant to energy storage applications. To this pursuit, a comprehensive analysis was realized by structural, morphological, mechanical, thermal, and electrical assessment, anticipating that the framework of the hydrophobic aromatic component functionalized with the polar nitrile group and the hydrophilic semi-aromatic Jeffamine substructure would enable high dielectric constant values as well as increased mechanical and electrical performance in energy storage.

Copolyimides synthesis and structural identification

All copolyimides reported here were obtained by classical two step polycondensation reactions between a mixture of two diamines in different molar ratios and BTDA. These implied first the formation of the intermediary copoly(amidic acids) and afterwards their conversion into the corresponding copolyimide structures by thermal imidization in solution. Thus, as shown in Scheme 1, three series of copolyimides were obtained: series 1, in which the molar ratio of aromatic diamine to aliphatic diamine was 0.7 : 0.3 (**coPI1–coPI3**), series 2, in which the same molar ratio was modified to 0.6 : 0.4 (**coPI4–coPI6**), and series 3 with an equal molar ratio between the two diamines (0.5 : 0.5, **coPI7–coPI9**). The copolymers containing polar nitrile groups in the main chains were obtained as viscous solutions at the final stage of the polycondensation process. Structural identification of these copolymers was performed by using FTIR and ^{1}H-NMR spectroscopies.

^{1}H-NMR spectra were discussed in correlation with the structural design of each copolyimide series, considering the ratio of aromatic and aliphatic segments in the macromolecular chains. The primary information provided by these spectra refers to the absence of the signals specific for the amide protons at about 13–15 ppm (carboxylic protons) and 9.5–9 ppm (amide protons), thus indicating a complete imidization of the copolymer intermediates to the corresponding copolyimide structures. According to Fig. 1, which shows the ^{1}H NMR

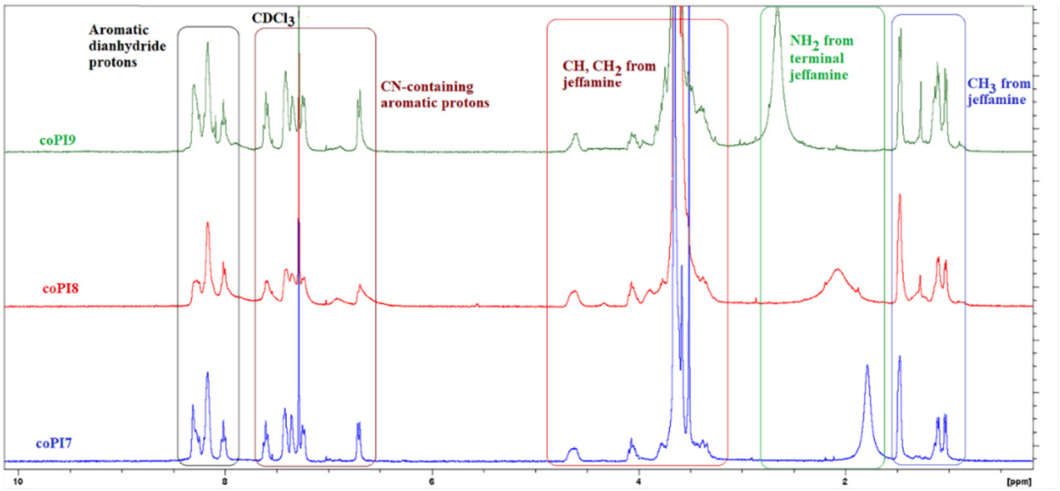

Fig. 1 ^{1}H-NMR spectra of copolyimides **coPI7**, **coPI8** and **coPI9** obtained from the equal molar ratio between the aromatic diamine and aliphatic diamine.

spectra for the copolyimide series 3 containing a 0.5 : 0.5 molar ratio between aromatic diamine and aliphatic diamine, the characteristic protons of the studied copolymers are scattered into four main regions. Thus, the signals identified at 8.30–7.97 ppm were assigned to the protons coming from the diimide segment, while the protons found in the range of 7.63–6.62 ppm were attributed to the nitrile-containing aromatic fragment. The aliphatic Jeffamine-derived substructure was identified through multiple peaks in the range of 4.64–3.57 ppm assigned to methylidene (–CH) and methylene (–CH_2) protons, and 1.76–0.96 ppm due to methyl (–CH_3) protons. An additional resonance signal in the form of a broad clear peak was observed in the high field range, between 2.66 and 1.78 ppm, for all investigated copolyimides, except **coPI4** and **coPI5** for which this peak had a lower intensity, as can be observed in Fig. S1 (ESI†). In previous work, a similar signal centered at about 1.75 ppm was recorded in the ^{1}H NMR spectrum ($CDC1_3$) of Jeffamine ED-600 and associated with its aliphatic amine protons.[31] Therefore, it appeared reasonable to attribute this signal to the NH_2 protons of the terminal Jeffamine (J-600, J-900 or J-2000). The broadness of the peak and the shift to different resonance fields suggest the involvement of the amine group in intermolecular interactions, particularly in H bonding, where it behaves as a proton donor towards a proton acceptor, which can be imide C=O or the bridged C=O in the diimide segment, as well as CN group. The reason why this band is of lower intensity for **coPI4** and **coPI5** is mostly due to the lower reactivity of BTDA compared to that of aromatic and aliphatic diamines mixture.

The ^{1}H-NMR technique was also used to evaluate the comonomer ratio on the basis of the integral area of the ^{1}H-NMR signals recorded at 7.63–6.62 ppm region corresponding to the aromatic diamine containing nitrile protons and from 4.64–3.57 ppm domain which were attributed to CH and CH_2 protons from the aliphatic diamine segment (Table S2, ESI†). The obtained results did not evidence a pronounced deviation from the initial target molar ratio. Still, a general trend can be observed in the case of copolymers **coPI3**, **coPI6** and **coPI9** containing the J-2000 fragment: the loading of the aromatic diamine is slightly higher than that of the aliphatic one, which suggests a better reactivity of the former diamine. Conversely, the incorporation of aliphatic diamines J-600 and J-900 into the corresponding copolymers occurred in higher amounts with respect to the targeted ones, while only **coPI5** had very close values to the predicted ones. In this context, the reactivity of aliphatic diamines with respect to the CN-based aromatic diamine appears different against BTDA in the polycondensation reaction: the higher the molecular weight of the Jeffamine, the lower the reactivity towards BTDA compared to the aromatic diamine.

The second analysis used to demonstrate the correct structure of the proposed copolyimides relied on FTIR spectroscopy. Since all designed copolymers are based on the same structural elements, and the only difference arises from the content variation of the aliphatic diamine-derived component and its chain length, the recorded spectra exhibited comparable features. Thus, the absorption bands generated by the newly formed imide cycle at 1780–1776 cm^{-1} and 1724–1711 cm^{-1} (assigned to symmetrical and asymmetrical stretching vibrations of carbonyl group), 1377–1367 cm^{-1} (attributed to C–N stretching) and 721–714 cm^{-1} (due to imide ring deformation) proved the success of the cyclodehydration process of the intermediate copoly(amidic acids). Also, FTIR spectra indicated that the functional groups coming from the starting monomers provided the corresponding absorption bands, as follows: nitrile unit, at 2233–2228 cm^{-1}, aromatic ether moiety (from the aromatic diamine segment) at about 1238–1234 cm^{-1}, the bridged carbonyl unit (belonging to the diimide segment) at 1672–1660 cm^{-1}, the asymmetric and symmetric methylene and methyl groups at 2943–2920 cm^{-1} and 2869–2853 cm^{-1}, the aliphatic C–O–C stretching and aliphatic C–O bending (belonging to the Jeffamine fragments) at about 1101–1091 cm^{-1} and 860–854 cm^{-1}, respectively (Fig. 2).

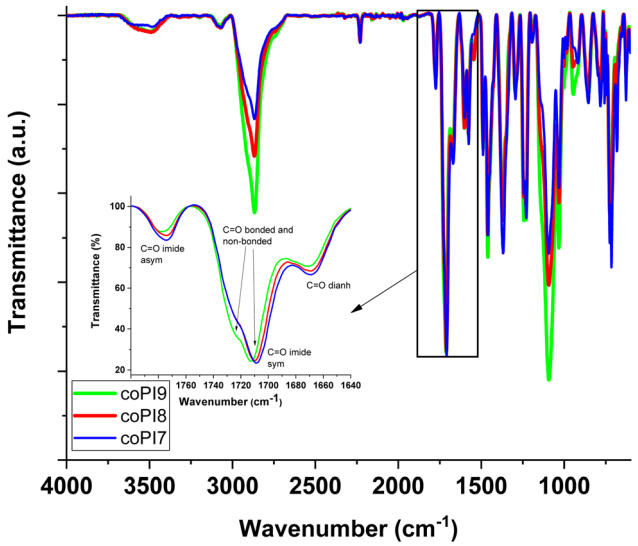

Fig. 2 FTIR spectra of copolyimides **coPI7**, **coPI8** and **coPI9** with a molar ratio of 0.5 : 0.5 of aromatic diamine to aliphatic diamine (inset: enlarged FTIR spectra across the 1800–1640 cm^{-1} region).

FTIR spectra also confirmed the ^{1}H-NMR hypothesis regarding the presence of hydrogen-bonded and non-bonded (free) NH_2 groups of the end Jeffamines. Thus, the occurrence of some broad absorption bands (more intense for those containing J-600 and J-900 segments) at about 3587–3550 cm^{-1} and 3363–3338 cm^{-1} attributed to free/bonded terminal Jeffamine amino groups and an obvious splitting of the absorption bands due to symmetric and asymmetric carbonyl imide stretching was noticed (Fig. 2). Although the CN group is also a potential H acceptor, no alteration of CN absorption band was noticed in comparison to that of the previously reported CN-containing polyimide.[30] Thus, intermolecular interactions through hydrogen-bonding involving imide carbonyl and terminal Jeffamine amine are anticipating, and hence a good miscibility of the hard and soft segments, as it will be further discussed.

Solubility, film-forming ability and molecular weight evaluation

The evaluation of the processability of the copolyimides was made by measuring the solubility at a concentration of 0.5% in a variety of high polar aprotic (NMP, DMSO, DMAc) and less-polar (THF, DCM, ACN, $CHCl_3$) solvents at room temperature. The results showed that these copolymers have excellent solubility in all solvents with some exceptions: in acetonitrile part of the samples swelled up, while the other part was soluble, while in chloroform and dichloromethane just the series with the molar ratio aromatic diamine : aliphatic diamine = 0.7 : 0.3 exhibited the same peculiarity, all other copolymers (**coPI4–coPI9**) being soluble (Table S3, ESI†). The swelling behavior of the copolyimides in low polarity solvents is similar to that of a semi-interpenetrating polymer network, owing to the formation of H bonds between soft and hard segments. It appears that the soft segments dissolute in these solvents and act as plasticizers for the hard segments, especially when these are loaded in higher amounts, thereby leading to the gel behavior of the polymers. These bonds mostly lose their stability in high polar solvents due to the higher ability of the amidic polar solvents to establish hydrogen bond interactions with the terminal Jeffamines units, as observed earlier.[29]

The processing characteristics of these copolymers in terms of film forming ability were tested in various solvents and at different concentrations, function of the solubility of each sample. In order to properly evaluate and compare the properties of the free-standing films, and to implement the easiest solvent removal protocol, THF was used as a solvent at a content of 10 wt% in solids, although good quality films were also obtained by using DMAc at a concentration of 20 wt%, but under more drastic conditions. The obtained free-standing films were flexible, or even stretchable, maintained their physical integrity at multiple bending, rolling, and in some cases behaved as self-sticky materials. An exception was encountered for **coPI9**, which exhibited the most self-sticky feature and a wax-type behavior, thereby impeding easy handling. However, regardless of the solvent or concentration used for film preparation, the self-sticky feature was noticed for all copolyimides derived from J-2000 when they got in touch with themselves or with silicone weighing paper (Fig. 3), while the sticky strength increased with the amount of J-2000 loading.

The measurements of the molecular weights were performed by GPC experiments by using copolymer powder dissolved in DMF solution. The values of the specific parameters, namely the number average molecular weight (M_n), the weight average molecular weight (M_w), and the polydispersity index (M_w/M_n) are listed in Table 1. As a first observation, the molecular weight values are consistent with those of the constituent Jeffamine aliphatic segment. Thus, M_n and M_w values increased with the rise of the molecular weight of the Jeffamine (J-600 < J-900 < J-2000), except for series 2 where a reverse order was observed. According to Table S2 (ESI†), this can be

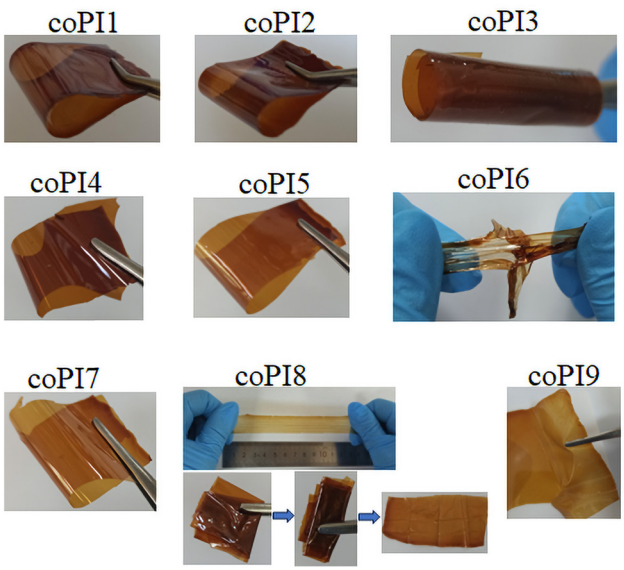

Fig. 3 Photographs of the copolyimide films **coPI1–coPI9**.

Table 1 Molecular weights, WAXD and AFM data of copolyimides **coPI1–coPI9**

Copoly-imides	M_n [g mol^{-1}]	M_w [g mol^{-1}]	M_w/M_n	*d*-sp [Å]	Sa [nm]	Sq [nm]
coPI1	171 500	301 300	1.76	4.58	0.44	0.56
coPI2	180 400	304 000	1.69	4.13	0.31	0.44
coPI3	187 600	311 800	1.66	4.29	0.17	0.21
coPI4	111 100	194 600	1.75	4.57	0.22	0.28
coPI5	100 900	186 200	1.85	4.36	1.06	1.57
coPI6	89 600	170 700	1.91	4.24	0.72	0.97
coPI7	76 700	147 000	1.92	4.48	0.92	1.16
coPI8	131 800	230 200	1.75	4.35	1.00	1.39
coPI9	170 800	301 700	1.77	4.28	0.48	0.67

M_n – the number average molecular weight, M_w – the weight average molecular weight, M_w/M_n – polydispersity index, Sa – average roughness, Sq – root mean square roughness.

attributed to the higher amount of J-600 incorporated into the copolymer compared to J-900, and especially to J-2000, being facilitated by the higher reactivity of J-600 against BTDA, which thereby compensates the contribution brought by the Jeffamine molecular weight. Still, the values obtained for these copolyimides are high, with M_n in the range of 187 600–89 600 g mol^{-1}, M_w between 304 000 and 170 700 g mol^{-1}, and a relatively low polydispersity (1.66–1.92). The overall data indicate a good reactivity of the selected monomers towards BTDA in the polycondensation reaction, which enabled the development of defect-free films *via* conventional solution casting methods.

Characterization of copolyimide films

Wide-angle X-ray diffraction (WAXD) studies. WAXD diffractograms were measured with the aim of evaluating the influence of the Jeffamine's variable content and molecular weight onto the solid-state packing ability of copolyimide films. The registered patterns exhibited broad halos with the maxima centered in the range of 19.59–21.16°, with no diffraction peaks characteristic to the crystalline domains of polyethylene oxide (Fig. S2, ESI†). This feature that can be attributed to amorphous copolymer structures with randomly distributed macromolecular chains is in a perfect agreement with the DSC experiments data, were no melting or crystallization peaks were observed for none of the investigated copolymers (see Thermal behavior section).

The average interchain spacing distance (*d*-spacing) was estimated in the range of 4.19–4.39 Å, similar to the ones obtained for related semi-aromatic copolyimides.[29] It was noticed that for each series of copolymers, the increase in the molecular weight of the constituent Jeffamine leads to a slight decrease of *d*-spacing value, except for **coPI3**. Though higher flexibility induced by the more voluminous aliphatic segment was expected to increase the free volume and the *d*-spacing, the effect was opposite. The decrease of the *d*-spacing as indicative of more tightly packed polymer chains suggests the involvement of Jeffamine segments in a polymer network that impedes a higher mobility, resulting in a low free volume. With the increase of the Jeffamine molecular weight, the strength of the network became higher as result of more intensive intermolecular interactions, leading to a reduced *d*-spacing. On the other hand, a comparison of the *d*-spacing values obtained for the copolyimide series based on the same Jeffamine incorporated in different amounts evidenced that a general rule cannot be drawn. However, it is clear that beside the length and quantity of the aliphatic sequence from the copolyimides, other factors like the ability of the terminal Jeffamine to develop H bonding, or polymer molecular weight contribute to the driving force that adjusts the chain packing of the studied polymers. Overall, their *d*-spacing values are lower when compared to other semi-aromatic copolyimides incorporating J-2000 segments,[32] thus supporting the existence of attractive forces between the soft and hard imide constitutive fragments, like in a polymer network, as demonstrated by rigid polyimides engaged in SIPN.[33]

Film morphology studies. The surface morphology of the copolyimides was explored by AFM technique which provided the 3D (Fig. S3, ESI†) and phase contrast (Fig. 4) images of the film surfaces, along with the average roughness (Sa) and root mean square roughness (Sq) parameters (Table 1). The obtained Sa and Sq parameters are generally characteristic of smooth surfaces and decrease with the rise of the Jeffamine chain length in the series derived from the molar ratio aromatic diamine: aliphatic diamine = 0.7 : 0.3. For the other two series,

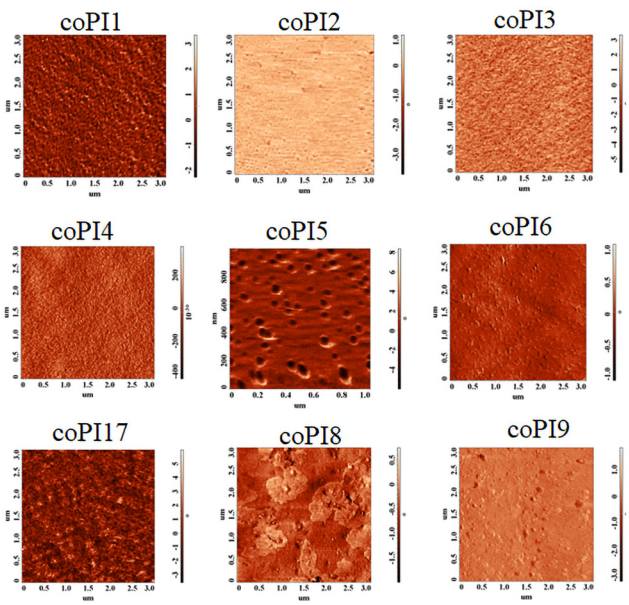

Fig. 4 Phase images of copolyimides **coPI1–coPI9**.

the trend is different, with roughness increase when passing from J-600 to J-900, and then decrease when passing from J-900 to J-2000. Such inhomogeneous variation suggests different arrangements of the hard and soft segments in the network, in dependence on the strength of intermolecular interactions developed by each polymer, in agreement with WAXD findings.

Further information on the developed network by each investigated polymer was obtained by recording the phase images (Fig. 4). There are some contradictory reports regarding the assignment of the copolymer components, with some of them assigning the darker phase areas (the more negative phase) to the soft component of the material,[34–36] and others to the hard component.[37–41] These inconsistencies are the result of different dynamic modes of AFM data acquisition, namely: soft tapping (when the ratio (r_{SP}) between the set-point tapping amplitude and the free amplitude is higher than 0.5), moderate tapping (when r_{SP} is around 0.5) and hard tapping (when r_{SP} is lower than 0.5). Thus, in the situation of moderate tapping, the bright regions in the phase images are attributed to the hard component and the dark regions to the soft one, while in hard tapping (this being also our case, r_{SP} varies between 0.2 and 0.3) the phase image's contrast is shifted.[42] Therefore, the brighter regions in these images (Fig. 4) were associated with the soft semi-aromatic segments (since Jeffamine possesses longer aliphatic ether backbones which are mechanically softer than ether aromatic backbones), while the darker ones were assigned to the stiff aromatic fragment of the copolyimides. According to Fig. 4, the bright spots are distributed uniformly throughout the surface, except **coPI5** and **coPI8**, ensuring a smooth morphology, which suggests that the two components of the copolyimides were mixed randomly, consequent with WAXD measurements.

The increase in roughness could be tentatively attributed to the difference in solubility of the two constituent copolyimides: the segment containing the stiffer aromatic part may exhibit poorer solubility toward THF and "precipitated" first on the resulting surface upon film formation, followed by the softer aliphatic fragment, which embedded into the first layer by intermolecular interactions, as observed earlier.[40] We assume that this phenomenon led to different surface textures including globular formation, depending on the nature of the constituent Jeffamine fragment. This feature is more obvious in the case of **coPI5**, **coPI6**, **coPI8** and **coPI9** (which contain a higher amount of Jeffamine with increased molecular weight), which match the bright top regions displayed in Fig. 4. Combining these assumptions with the technical data obtained from the topographical 3D-surface texture and phase images, the generation of more pronounced topological textures as the Jeffamine ratio increased seems rational.

According to AFM data, the phase separation of the understudy copolyimides is not obvious, since the contrast variation is less than 12°, proving an efficient miscibility and interpenetration of the hard and soft imide components at the molecular level. Also, in DSC experiments, a single T_g was found without any melting or crystallization peaks, which also supports our statement of having amorphous copolymers with random distribution of the two components.

Mechanical properties. The free-standing copolyimide films prepared from **coPI1–coPI9** were first evaluated by visual assessment. Thus, the films features were found in close correlation with the quantity and nature of the Jeffamine aliphatic segment. In the case of **coPI1**, **coPI4** and **coPI7** (based on J-600) as well as **coPI2** and **coPI5** (incorporating J-900), the films enabled facile handling, were tough and flexible, even after repeated bending, when their physical integrity was maintained (Fig. 3). Other copolyimides that incorporated higher molecular weight J-2000 segments (**coPI3**, **coPI9**) or a higher amount of J-900 fragments (**coPI8**) were also flexible, and in addition stretchable, these features being predominant mostly in the case of **coPI8** and **coPI9** who exhibited an increased self-sticky behavior. Furthermore, **coPI9** evidenced a difficult handling since its adhesion to the Teflon surface was very strong, which impeded further mechanical test investigations. Such characteristics may be attributed to the adhesion forces evolved as a consequence of the intermolecular interactions with a support, or due to cohesive forces between the macromolecular chains, as observed in related copolyimides.[29]

Uniaxial and cyclic tensile tests were further performed in order to establish an appropriate quantitative mechanical evaluation of the copolyimide films. Accordingly, the stress–strain curves are shown in Fig. 5(a) and (b), while the main parameters are listed in Table 2.

An overall view of the obtained data reveals that the most important factors which tailor the mechanical behavior of the copolymer films are represented by the nature (J-600, J-900 or J-2000) and the quantity (0.3, 0.4 or 0.5 molar ratio) of the Jeffamine segment in the main chain.

The data were discussed considering each series of copolymers derived from the same molar ratio of different Jeffamines. In terms of strain at break, the highest value in each series was recorded for the copolyimide incorporating the longest aliphatic chain *e.g.* J-2000 (427% for **coPI3** and 469% for **coPI6**), being followed by the copolyimide series based on J-900 (130% for **coPI5** and 410% for **coPI8**). All these films display a large stretching ability upon applied stress, a feature which is scarcely encountered in classical aromatic polyimides. Accordingly, the nature and quantity of the Jeffamine appear to have a profound effect on this parameter. In this regard, please also note the tremendous difference recorded for the copolymers containing J-2000 and J-600 fragments, with the latest behaving as very rigid polymers (1.9% for **coPI1**, 0.9% for **coPI4** and 1.9% for **coPI7**). It is clear that the increase of the molecular weight and the quantity of the aliphatic component leads to a significant rise of the deformation at a break in all 3 series. This variable behavior can be the result of intermolecular interactions inside the generated polymer network, between the thermoplastic aromatic segment and the rubber-type semi-aromatic fragment, without excluding the interactions developed inside each copolymer component. We assume that J-2000 segments enable increased packing ability, as demonstrated by the lower values of *d*-spacing, which promotes facile chain sliding inside the network tie-point sites. J-600 definitely triggers the generation of a network with a reduced extent, leading

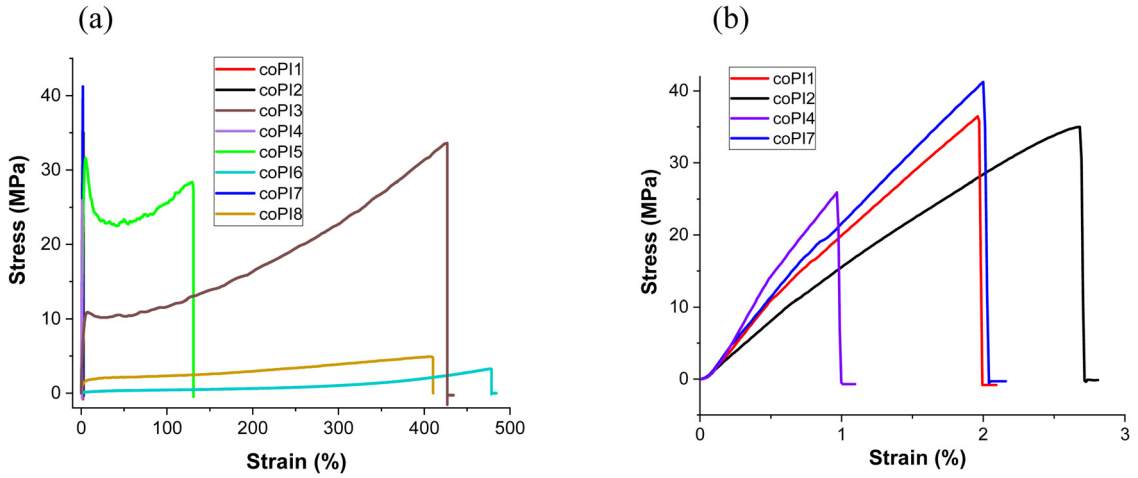

Fig. 5 (a) Strain–stress curves of copolyimides **coPI1–coPI8**; (b) enlarged stress–strain curves of copolyimides **coPI1**, **coPI2**, **coPI4** and **coPI7**.

Table 2 Mechanical parameters of copolyimides **coPI1–coPI8**

Copoly-imide	Strain at break, %	Ultimate tensile strength, MPa	Young's modulus,[a] GPa	Toughness, MJ m^{-3}	Recovery strain at 100% strain, %
coPI1	1.9	38.3	2.301	0.40	N/A
coPI2	2.6	35.0	1.614	0.52	N/A
coPI3	427	33.6	0.404	79.50	18.44
coPI4	0.9	25.9	2.850	0.12	N/A
coPI5	130	28.3	1.197	32.23	N/A
coPI6	469	3.4	0.006	5.28	59.71
coPI7	1.9	34.3	1.893	0.36	N/A
coPI8	410	4.8	0.122	12.92	20.33

[a] Young's modulus determined at 0.5% strain.

to lower values of strain at break and higher interchain distances (see Table 1).

The ultimate tensile strength had a reverse trend as compared to strain at break, while the influence of Jeffamine nature on this parameter was not so profound. Generally, it was observed that with the increase of the molecular weight and quantity of the Jeffamine component, the ultimate tensile strength values decreased, with some exceptions. As expected, this parameter was higher for copolyimides containing shorter J-600 fragments or lower content of Jeffamines (**coPI1–coPI3** and **coPI7**), whilst at the increase of the semi-aromatic content the force necessary to break the films decreases rapidly, as evident in the case of **coPI6** (3.4 MPa) and **coPI8** (4.8 MPa). This is mainly due to the reduced amount of aromaticity which usually endows polymers with mechanical strength.

The stiffness of the copolymer chains was also evaluated on the basis of Young's modulus values. The obtained data correlate well with the length and quantity of the Jeffamine segment incorporated into the main chains. The trend was similar to that observed for the tensile strength, the highest values being recorded for copolyimides containing shorter, slightly stiffer J-600-based semi-aromatic fragments, and the lowest when more flexible J-2000 segments were incorporated into the chains.

The toughness, a mechanical parameter used to evaluate the ability of the copolyimide to absorb energy before breaking recorded the highest values for **coPI3** (79.50 MJ m^{-3}) and **coPI5** (32.23 MJ m^{-3}) which contain J-2000 and J-900 segments, respectively, in different proportions. It seems that the incorporation of longer aliphatic Jeffamine chains, or of a higher content of Jeffamine units is beneficial up to a limit, when other factors exert the influence and prevail, thus making difficult to draw any general conclusion. The obtained data emphasize a kind of synergism developed by the hard aromatic fragment with the soft Jeffamine segment when it is longer or shorter but in higher amounts, which is specific for each system. This is more evident for **coPI3**, which exhibited the highest toughness reported till now for semi-aromatic copolyimides. Thus, the ability of the soft and hard segment to arrange in the polymer network can lead to variable, distinct mechanical properties.

The viscoelastic behavior of the free-standing films to repeated deformation tests was evaluated for the copolyimides which recorded the highest values of strain at break (**coPI3**, **coPI6** and **coPI8**) by applying eight progressive loading–unloading cycles. According to Fig. 6a–c, all copolymers exhibited large hysteresis loops even at small strains, while most of the tensile strain is irreversible in the case of **coPI3** and **coPI8**. The cyclic stress–strain curves evidenced that with the rise of the strain amplitude in each cycle, the hysteresis loop showed a pronounced feature. The mechanical features were better emphasized when

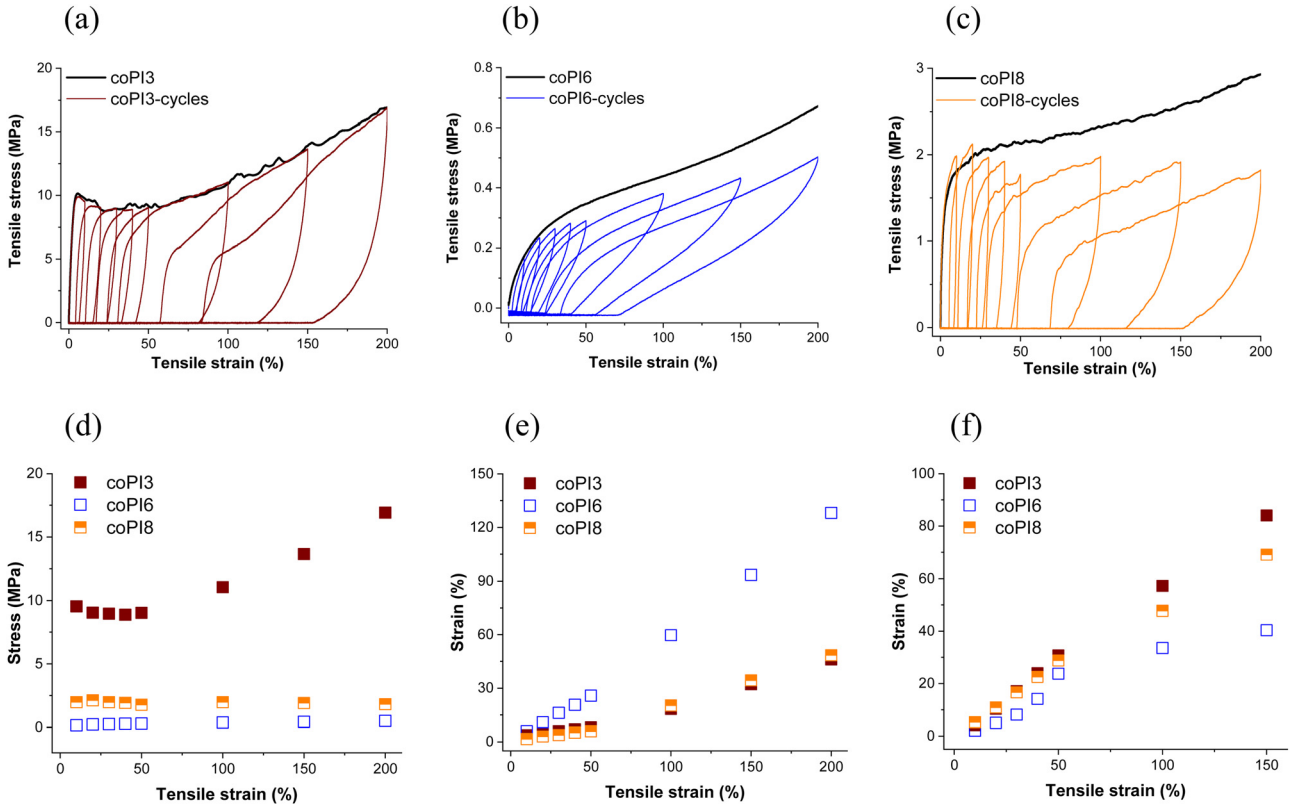

Fig. 6 Tensile stress–strain curve along with the obtained progressive loading curves for copolyimide (a) **coPI3**, (b) **coPI6**, and (c) **coPI8**. Variation of (d) maximum stress, (e) recovery strain and (f) permanent deformation corresponding to each loading cycle of **coPI3**, **coPI6** and **coPI8**.

the tensile strength of each loading–unloading cycle was plotted as a function to the applied strain (Fig. 6d). Different trends were noticed for the studied copolymers, as follows: **coPI3** recorded a small decrease in the first four cycles (40% strain) after which it increased until the rupture, for **coPI6** the maximum stress for each loading–unloading cycle increased monotonically with the applied strain, while **coPI8** recorded an almost constant tensile strength regardless of strain amplitude.

The recovery strain after unloading and the permanent deformation before reloading increased almost linearly with the applied strain (Fig. 6e and f). Copolyimide **coPI6** recorded the largest recovery strain and the lowest permanent deformation for each applied strain. Thus, at 10% strain, **coPI6** recorded a permanent deformation of 2.08% and a recovery strain of 5.83, while at 100% strain it disclosed a permanent deformation of 33.57% and a recovery strain of 59.71%, endowing this polymer with the best mechanical properties among the studied polymers, which is superior even to the related copolyimides previously reported by us.[29] It can be assumed that the increase of the molecular weight of the Jeffamine component was beneficial in the case of series 1 and 2, since the result obtained for **coPI8** from series 3 is lower as compared to **coPI6** from series 2.

Thermal behavior. The correlation between structure variation and thermal stability of the copolyimide films was made on the basis DSC and TGA data corroborated with the molar ratio between the two constitutive diamines and the molecular weight of the incorporated Jeffamine (J-600, J-900 or J-2000).

DSC studies. DSC curves (Fig. S4, ESI†) revealed a single glass transition for all studied copolymers without any crystallization or melting peaks, thereby informing on the absence of phase separation between the soft Jeffamine-imide fragment and the hard nitrile-aromatic-imide segment, and consequently the amorphous nature of the copolyimides. Generally, in phase separated polyimides, soft Jeffamine segments of the copolyimides should have a T_g between −54 to −59 °C,[43,44] while a T_g of about 226 °C was displayed by the hard aromatic-imide component.[30] Accordingly, due to the lack of two different T_gs no phase segregation occurred in our polymers. Since the incorporation of higher quantities of Jeffamine units may lead to a crystallization process, a special attention was focused on **coPI3**, **coPI6** and **coPI9** containing J-2000 sequences in various molar ratios. Still, except for the lower values of glass transition temperature (T_g) at an increased content of J-2000, no other particularities were recorded for these samples. Concerning the T_g values, an obvious trend was noticed: the increase in the Jeffamine molecular weight, as well as of its molar ratio resulted in a decrease of T_g (Table 3 and Fig. S4, ESI†). Thus, higher values of T_g were obtained for copolymers from the series derived from the molar ratio aromatic diamine: aliphatic diamine = 0.7 : 0.3. Also, the copolyimide based on J-600 units registers the highest value of T_g, being followed by the series based on J-900.

The longer aliphatic chains of J-2000 or the higher loading of a Jeffamine into the copolymer structures enabled a higher

Table 3 Thermal properties of copolyimides **coPI1–coPI9**

Copoly-imides	T_g [°C]	T_{onset} [°C]	T_{max1} [°C]	T_{max2} [°C]	T_{max3} [°C]	W_{700} [%]
coPI1	104	399	434	487	609	42.8
coPI2	64	392	425	505	633	39.3
coPI3	−20	376	411	487	583	37.0
coPI4	72	398	437	514	603	37.5
coPI5	20	394	425	501	619	33.1
coPI6	−33	377	412	506	—	32.0
coPI7	49	398	433	494	604	32.4
coPI8	5	382	416	520	705	41.6
coPI9	−36	382	414	519	689	30.5

T_g = glass transition temperature; T_{onset} = initial decomposition temperature; T_{max} = temperature of the maximum decomposition temperature; W_{700} = residue at 700 °C.

mobility of the soft fragment leading to a decreased T_g. Though T_g values of copolyimides containing J-2000 segments are below room temperature (**coPI3** = −20 °C, **coPI6** = −33 °C and **coPI9** = −36 °C), the other samples registered positive values of T_g, suggesting that from the chain mobility point of view, the molecular weight of the constitutive aliphatic segment surpasses the influence of the molar ratio. A comparison with the reported T_g data on related polyimides evidenced a good agreement in regard to both Jeffamine molecular weight and molar ratio between the aromatic and aliphatic diamines.[29,45–47]

Thermogravimetric measurements. The thermogravimetric analysis (TGA) of copolyimides performed in an inert atmosphere on free-standing films revealed a dependence on the aliphatic Jeffamine segment, similar to DSC measurements. First, a small initial weight loss (<2 wt%) was recorded for all copolyimides, in the range of 45–160 °C, which may be associated with the loss of adsorbed water and residual NMP solvent entrapped in these films. After corrections, the initial decomposition temperature (T_{onset}) was recorded within 376–399 °C. The decomposition process exhibited a weight loss pattern consisting of three consecutive steps. The first one (T_{max1}), at temperatures between 411–437 °C, was attributed to the loss of the soft part of the copolymers which contain the less thermally stable aliphatic Jeffamine fragments, while the second step (T_{max2}) at about 487–520 °C and the third one (T_{max3}) in the range of 583–705 °C, with a lower mass loss were assigned to the scission of flexible linkages and decomposition of the remaining hard aromatic part of the copolyimide backbone, respectively (Fig. 7). The weight residue of copolyimides **coPI1–coPI9** found at 700 °C (W_{700}) had values within 30.53–42.8%, which is consistent with the quantity of the constitutive hard aromatic imide fragment from each macromolecular backbone (Table 3).

By analyzing the data obtained from TGA, a correlation with copolymers composition can be drawn. As a general trend, with the increase of molecular weight and/or of the molar ratio of the incorporated Jeffamine, the thermal parameters (T_{onset}, T_{max} and W_{700}) followed the order: series 1 > series 2 > series 3. Thus, for copolyimides based on the same Jeffamine but belonging to different series, the higher the quantity of the aliphatic segment, the lower the thermal resistance.

The thermal stability obtained for **coPI3**, **coPI6** and **coPI9** is higher than that of reported copolyimides based on pyromellitic dianhydride, 3,3′,4,4′-biphenyltetracarboxylic dianhydride or BTDA, and 4,4′-oxydianiline and J-2000 (weight ratio aliphatic diamine: aromatic diamine = 1 : 1, 2 : 1 or 4 : 1) (T_g = −57 to −42 °C, T_{onset} < 300 °C and T_{max1} = 360–380 °C),[48] or other copolyimides obtained from 6,13-bis(4-amino-2-trifluoromethylphenoxy)pentiptycene, J-600, J-900 or J-2000 and 4,4′-hexafluoroisopropylidene bisphthalic dianhydride (in Jeffamine

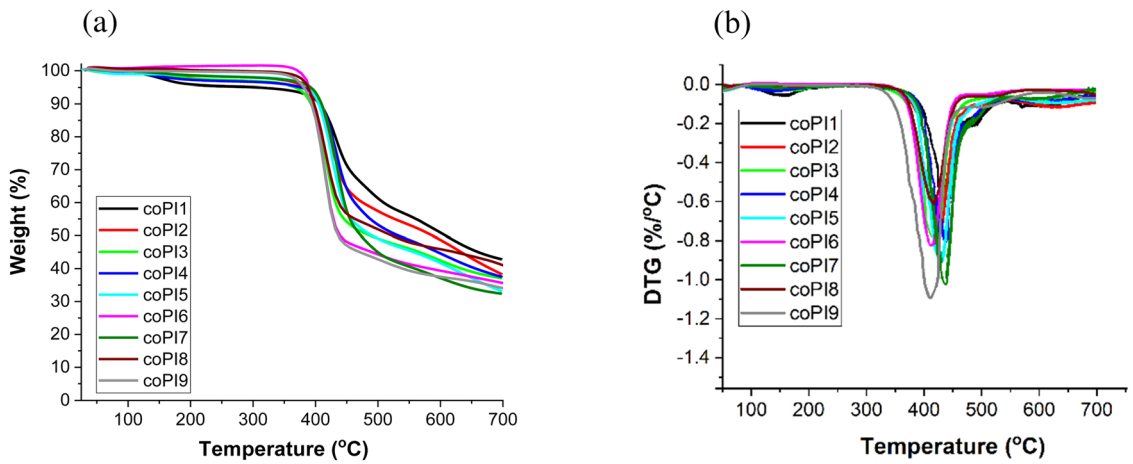

Fig. 7 (a) TG and (b) DTG curves of **coPI1–coPI9**.

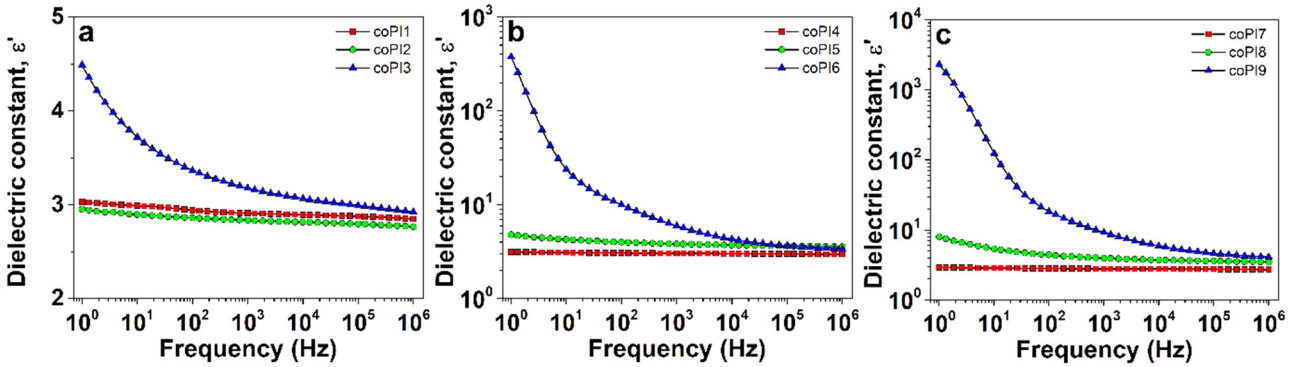

Fig. 8 The evolution of dielectric constant with frequency at room temperature for copolyimides with (a) 0.7 : 0.3, (b) 0.6 : 0.4 and (c) 0.5 : 0.5 molar ratio.

Table 4 The values of dielectric constant, dielectric loss and conductivity at room temperature and at frequencies of 1 Hz and 1 kHz

	Dielectric constant, ε'		Dielectric loss, ε''		Conductivity, σ (S cm^{-1})	
Copoly-imide	f = 1 Hz	f = 1 kHz	f = 1 Hz	f = 1 kHz	f = 1 Hz	f = 1 kHz
coPI1	3	2.9	0.04	0.02	2.2×10^{-14}	8.7×10^{-12}
coPI2	2.9	2.8	0.06	0.02	2.1×10^{-14}	8.6×10^{-12}
coPI3	4.5	3.2	1.8	0.1	9.8×10^{-13}	5.6×10^{-11}
coPI4	3.1	3	0.04	0.01	2.1×10^{-14}	7.7×10^{-12}
coPI5	4.8	3.8	0.6	0.09	3.5×10^{-13}	5.0×10^{-11}
coPI6	376	6	2355	4.4	1.3×10^{-9}	2.4×10^{-9}
coPI7	2.9	2.8	0.06	0.02	3.1×10^{-14}	8.9×10^{-12}
coPI8	8	3.9	5.8	0.2	3.2×10^{-12}	1.3×10^{-10}
coPI9	2294	9.2	7150	13.2	4.0×10^{-9}	7.3×10^{-9}

weight percent of 40 and 50%) (T_g = −18 to 65 °C, T_{onset} = 343–369 °C and T_{max1} = 520–530 °C).[49] These attributes are likely due to the arrangement of our polymer chains in polymer networks, perhaps facilitated by the presence of the CN group. Overall, the data obtained here show a high thermal resistance (T_{onset} > 376 °C) of all copolyimides, which is typical for thermostable polymers with potential use in electronic devices where heat is generated during operation.

Broadband dielectric spectroscopy (BDS) measurements

The isothermal BDS plots of the dielectric constant (ε') parameter as a function of the electrical field frequency (f) at room temperature were recorded for each series of copolyimides and displayed in Fig. 8. In addition, the $\varepsilon'(f)$ profiles of copolyimides derived from the same Jeffamine are comparatively shown in Fig. S5 (ESI†). Table 4 lists the dielectric constant values selected at various frequencies and at room temperature.

According to Fig. 8, ε' has a low magnitude, revealing a reduced dipolar activity for **coPI1–coPI3** copolymers containing the lowest molar ratio of aliphatic diamine, while a noticeable enhancement of ε' amplitude was recorded at the Jeffamine content increase (**coPI4–coPI6** and **coPI7–coPI9** copolyimides), suggesting an improved dipolar activity. A spectacular increase of this parameter was noticed for copolyimides based on J-2000 segments, especially at higher loading (**coPI6** and **coPI9**) and low frequency (Table 4), providing clear evidence for the effect of aliphatic segments on the copolymer dielectric characteristics. On the other hand, the $\varepsilon'(f)$ profiles of copolyimides exhibited two different behaviors: (i) a slight decrease of ε' towards increasing frequency (for copolyimides based on J-600 and J-900, as shown in Fig. S5a and b, ESI†) and (ii) a considerable drop of ε' noticed especially at low frequencies (for copolyimides based on J-2000, as shown in Fig. S5c, ESI†). This feature may be attributed to the electrode polarization effect induced by the accumulation of charge carriers at interfaces between the sample surfaces and the BDS electrodes used for dielectric measurements.[50]

The isothermal BDS plots of ε' as a function of frequency at various temperatures are exemplarly shown for **coPI4** and **coPI6** in Fig. 9. At low temperatures, ε' has a reduced amplitude which decreases slightly with increasing frequency due to low dipolar activity. As temperature increases, the dipoles of the macromolecular chains gain a sufficient thermal energy and, consequently, enhance the ε' amplitude, with a concomitant decrease towards increasing frequency. In the case of the copolyimide based on J-2000 segment, the polarizable units are thermally activated at significantly lower temperatures (Fig. 9b, $\varepsilon'(f)$ profile around 0 °C) compared to those of the J-600-based copolyimide (Fig. 9a, $\varepsilon'(f)$ spectrum around 100 °C).

To better evaluate the effect of temperature on the dielectric behavior of our copolyimides, ε' was plotted against temperature at a fixed frequency, of 1 kHz, as presented in Fig. 10. Thus, two different regions were identified: (i) a low temperature region, where ε' varied slightly with temperature and (ii) a high-temperature region, where ε' substantially enhanced with temperature increase. The rise of ε' in the second region can be

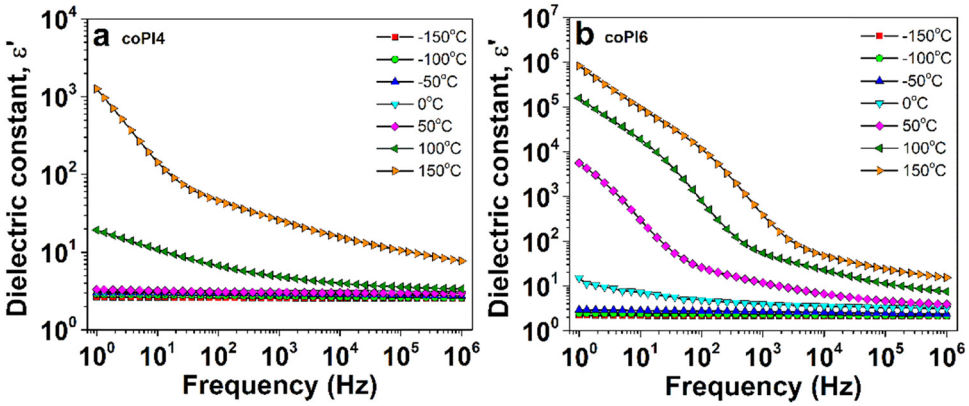

Fig. 9 The evolution of dielectric constant with frequency at various frequencies for (a) **coPI4** and (b) **coPI6** copolyimides.

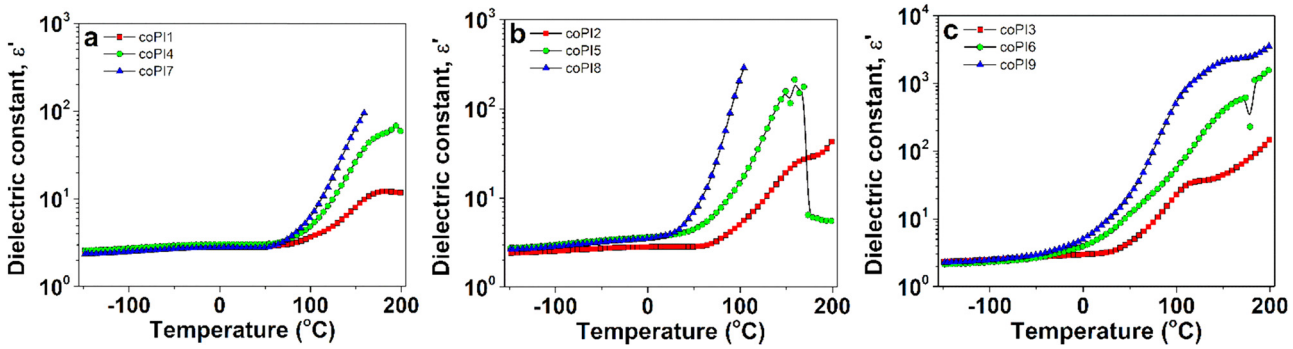

Fig. 10 The evolution of dielectric constant with temperature at 1 kHz for copolyimides containing (a) J-600, (b) J-900 and (c) J-2000 Jeffamines.

corelated with the glass transition temperature of the materials, being associated with segmental motions of polymer backbone.[51] As expected, the copolyimides based on J-600 segment recorded the highest T_g values among all the investigated copolyimides, and, consequently, the transition between the dielectric regions is delayed above *ca.* 70 °C. For copolyimides containing J-2000 sequences, the rise of ε' in the second region is promoted below 0 °C. Following this remark, it may be concluded that the dielectric constant values from Table 4 discussed previously are strongly dependent by the physical state experienced by copolyimide during heating.

The frequency dependencies of dielectric loss, another important parameter for electrical applications of polymers, are displayed in Fig. 11 and Fig. S6 (ESI†). From the curve profiles, it was clear that the dielectric loss parameter increased with the rise of the aliphatic diamine content. The lowest dielectric losses (*e.g.* >0.1 in the entire frequency range) were obtained for copolyimides with J-600 segments, which followed a gradual increase trend with the rise of the molecular weight of Jeffamine (Fig. S6, ESI†).

The conductivity evolution of the copolyimides with frequency at room temperature was further evaluated (Fig. 12). As generally

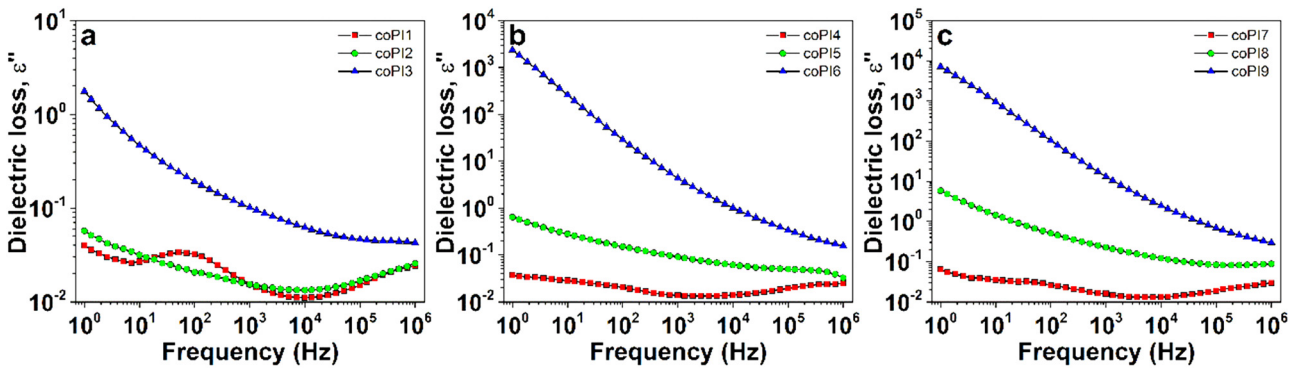

Fig. 11 The evolution of dielectric loss with frequency at room temperature for copolyimides with (a) 0.7 : 0.3, (b) 0.6 : 0.4 and (c) 0.5 : 0.5 molar ratio.

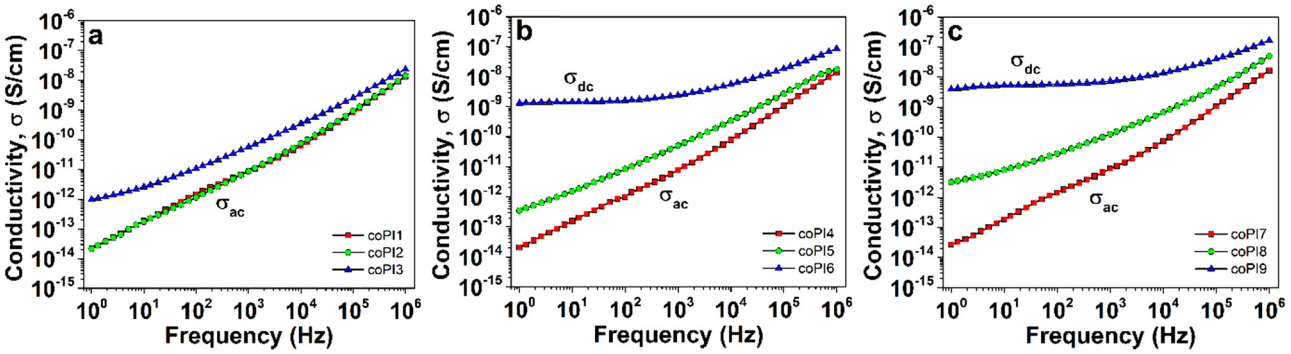

Fig. 12 The evolution of conductivity with frequency at room temperature for copolyimides with (a) 0.7 : 0.3, (b) 0.6 : 0.4 and (c) 0.5 : 0.5 molar ratio. The linear increase of conductivity corresponds to σ_{ac}, whereas the flat plateau region assigns with σ_{dc}.

known, the conductivity parameter may be expressed as the sum of ac-conductivity (σ_{ac}) and dc-conductivity (σ_{dc}), which can be differentiated from the isothermal plot shapes.[29] Thus, the regime of linear increase in conductivity against frequency is characteristic to ac-conductivity component and attributed to relaxation phenomena of the material. On the other hand, the region where conductivity is independent of frequency is an indicative of dc-conductivity, which is consistent with the transport of free charge carriers through the material.[52]

As shown in Fig. S7a (ESI†), the copolyimides based on J-600 exhibited exclusively an ac-conductivity, with values around 10^{-14} S cm^{-1} at 1 Hz. Considering the copolyimides derived from higher molecular weight Jeffamines, the frequency dependence of conductivity was substantially changed (Fig. S7b, ESI†). Thus, at low frequencies, the conductivity deviates from the linear increase, announcing the rise of the dc-conductivity regime. As consequence, the values of conductivity range between $\sim 10^{-14}$ S cm^{-1} for copolyimide with 0.7 : 0.3 molar ratio to $\sim 10^{-12}$ S cm^{-1} for copolyimide with 0.5 : 0.5 molar ratio between aromatic and aliphatic diamines (Table 4). An important enhancement of conductivity was noticed for copolyimides incorporating J-2000, up to $\sim 10^{-9}$ S cm^{-1}, especially in the case of **coPI6** and **coPI9**. Accordingly, these two polymers can support the transport of free charge carriers.

Electrical breakdown strength and energy storage density

The insulating ability of the copolyimide films was explored by means of electrical breakdown strength (E_{BD}) measurements. Because the present free-standing films are meant to be used in electrical and electronic applications (*e.g.* integrated circuits, thin-film capacitors, flexible/stretchable substrates, *etc.*), the failure behavior under electrical stress is of crucial importance since it may cause permanent deterioration of the insulating material. There are multiple factors which could influence the electrical breakdown strength of polymers, including molecular weight, cross-linking, crystallinity, molecular motion, chemical structure of the dielectric polar groups, along environmental aspects. Therefore, in the view of using dielectric polymer materials in thin film capacitors for energy storage purposes, several issues still need to be solved, which require deeper studies on this subject.

To evaluate the electrical stability of the copolyimide films, the Weibull distribution was employed based on the measured electrical breakdown strength values (Fig. 13a–c). The Weibull cumulative distribution function, $F(E_{BD})$, is defined by the following equation:

$$F(E_{BD}) = 1 - \exp\left[-\left(\frac{E_{BD}}{\alpha}\right)^{\beta}\right]$$

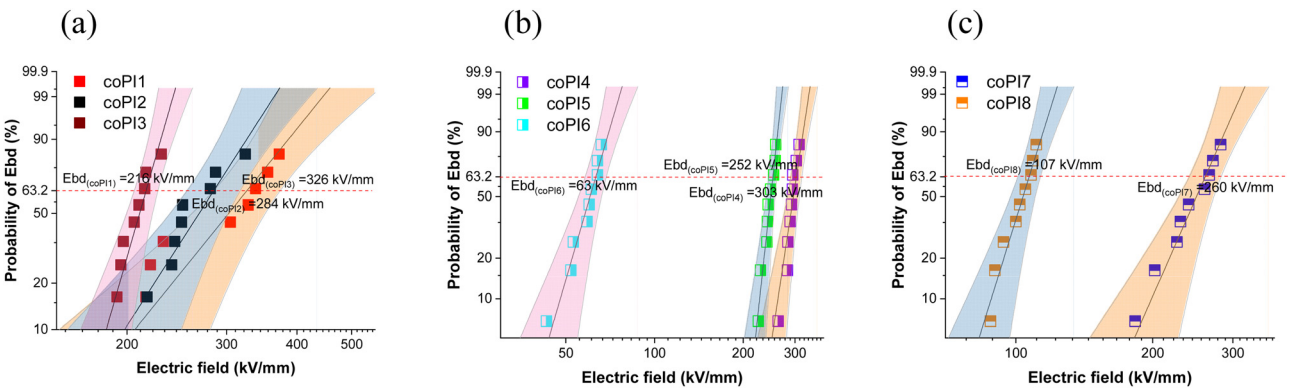

Fig. 13 Weibull distribution of dielectric strength for: (a) series 1 (**coPI1**, **coPI2** and **coPI3**), (b) series 2 (**coPI4**, **coPI5** and **coPI6**) and (c) series 3 (**coPI7** and **coPI8**).

Table 5 Weibull parameters of electrical breakdown tests of copolyimides **coPI1–coPI8**

Copoly-imide	Weibull scale parameter η (kV mm^{-1}), 95% confidence interval	Weibull shape parameter β, 95% confidence interval	Energy storage density, J cm^{-3}
coPI1	326 [284 < η > 373]	4.9 [2.8 < β > 8.5]	1.36
coPI2	284 [255 < η > 317]	6.1 [3.7 < β > 10.2]	1.00
coPI3	216 [206 < η > 226]	13.8 [8.3 < β > 23.0]	0.66
coPI4	303 [290 < η > 316]	15.6 [9.5 < β > 25.4]	1.22
coPI5	252 [244 < η > 260]	21.7 [12.7 < β > 36.8]	1.07
coPI6	63 [58 < η > 68]	8.1 [4.7 < β > 13.7]	0.11
coPI7	260 [240 < η > 282]	8.2 [4.8 < β > 14.3]	0.84
coPI8	107 [101 < η > 113]	11.7 [6.9 < β > 19.8]	0.20

in which α represents the scale parameter and is the electric field at which 63.2% of the measurements lead to the electrical breakdown, and β expresses the shape parameter, also named Weibull modulus, that indicates the width of the distribution.[53] With the increase of β parameter, the distribution width of the breakdown becomes smaller. The value of the location parameter was set to 0, which shows that the material may fail as soon as the voltage is applied.[54] The Weibull distribution parameters (α and β) and the linear fits for copolyimide **coPI1–coPI8** are listed in Table 5.

The Weibull scale parameter (E_{BD}) values demonstrated that there are significant differences between the 3 synthesized series of copolyimides in terms of electrical breakdown strength. As expected, the values of E_{BD} are dependent on the length of the Jeffamine segment. Thus, in each series for copolymers, higher values of E_{BD} were obtained for copolyimides containing shorter J-600 Jeffamine fragments, followed by the ones incorporating J-900 and J-2000 segments, respectively.

Also, the reinforcing effect of the aromatic component of the copolyimide is clearly observed since the highest values of E_{BD} were obtained for copolymers with an increased amount of hard aromatic segment (E_{BD} of **coPI1** > **coPI2** > **coPI3**). Still, the variation in E_{BD} is not so drastically altered by the quantity of the semi-aromatic component, as it is by the increased loading of higher molecular weight Jeffamines. This leads to a reduction of E_{BD} values as can be noticed for the second series, and moreover for the third series of copolymers, in good agreement with conductivity and dielectric data of copolyimides listed in Table 4.

Energy storage density evaluation. The energy storage performance of a dielectric material is characterized by the energy storage density (Ue) value.

By using the ε' data at 1 kHz (listed in Table 4) and the E_{BD} values (listed in Table 5), the energy storage density of **coPI1–coPI8** was found to be between 0.11 and 1.36 J cm^{-3}. Since higher values of both dielectric permittivity and breakdown strength are necessary to obtain increased Ue values, the obtained data emphasize the influence of the chemical structure of the constitutive structural elements on this parameter. Thus, overall increased Ue values were achieved for copolymers containing higher amounts of aromatic hard segments and the same J-600 Jeffamine (the Ue value of **coPI1** is higher than the one of **coPI4** and **coPI7**), either for those containing shorter aliphatic Jeffamine inside each series (**coPI1** > **coPI2** > **coPI3** in the first series, **coPI4** > **coPI5** > **coPI6** in the second series).

A comparison with the available reported data highlighted that the energy storage performance of the present copolymers is higher than in the case of similar copolyimides (Ue = 0.221–1.092 J cm^{-3}),[29] Kapton (Ue = 0.59 J cm^{-3}),[55] related polyimide containing two nitrile units (Ue = 1.02 J cm^{-3}),[25] and comparable or even higher than the ones reported for commercially widely used biaxially oriented polypropylenes (BOPP) ($\approx$1.2 J cm^{-3}).[56] Still, the storage ability of our polymers is inferior to polyimides incorporating bipyridyl units (Ue = 2.77 J cm^{-3}),[27] sulphonyl (Ue = 7.04 J cm^{-3}),[26] or polymer blend based on Matrimid 5218 and Ultem 1000 (Ue = 8 J cm^{-3}),[7] due to a different structural approach.

However, taken into consideration the strategies involved towards increasing the electrical breakdown strength and dielectric constant, it can be concluded that the synergism between the soft semi-aromatic component and the hard aromatic segment into the copolyimide chains was beneficial.

Conclusions

Structural manipulation of three series of copolyimides was approached by integrating polar nitrile and carbonyl units in the hard segment along with Jeffamines of different molecular weights in the soft fragment, aiming to develop dielectric materials with variable physico-chemical properties by starting always from the same constituent monomers. The structural characterization of the copolymers enabled, beside the confirmation of the chemical design, the evidence of a polymer network formation with a specific arrangement for each copolyimide, thereby leading to particular behaviors. The obtained free-standing films were flexible or stretchable in the case of copolyimides with a higher amount of Jeffamine units, the highest strain at break value being 426% and the recovery strain being 59.71% for copolymers with a molar ratio of 0.4 : 0.6 aliphatic : aromatic diamines. The film morphology was characteristic of smooth surfaces without phase separations, although different arrangement of the hard and soft segments in the copolymer chains enabled various 3D surface topologies. WAXD and DSC measurements offered evidence for the amorphous nature of copolymers, without any crystallization peak or phase separation. Also, a single glass transition

temperature, in the range of -36 ± 104 °C, was recorded, showing that from the chain mobility point of view, the molecular weight of the constitutive aliphatic segment surpassed the influence of the molar ratio. The copolyimide films exhibited a high thermal stability, with initial decomposition temperatures above 377 °C, the overall thermal parameters being shaped by the nature of the semi-aromatic segment. The dielectric constant varied from 2.8 to 9.2 at 1 kHz, in close correlation with the nature and quantity of the Jeffamine groups. The highest value of breakdown strength (326 kV mm^{-1}) was obtained for the copolyimide containing the highest amount of hard aromatic segment and the Jeffamine with the lowest molecular weight, with a corresponding energy density storage of 1.36 J cm^{-3}. While the incorporation of Jeffamine segments had a meaningful effect on the overall copolyimide properties, a slight variation in the copolymer composition tailored these properties in large limits, changing the material from a rigid to a flexible one, or even stretchable, from a common material, to one with self-sticky ability, from a low-*k* to a high-*k* material, all these being possible by a straightforward strategy implying structural elements manipulation. Still, for practical applications in flexible/stretchable electronics such as energy storage capacitors or dielectric materials, it is still necessary to face the trade-off between mechanical and electrical performances, a reason that prompts us to fill this gap in the future.

Author contributions

I. Butnaru: conceptualization, formal analysis, data curation, investigation, methodology, funding acquisition, writing – original draft, and writing – review & editing; A.-P. Chiriac: formal analysis, investigation, and methodology; M. Asandulesa: BDS analysis and editing; C. Tugui: mechanical and EBD analysis and editing; I. Stoica: AFM analysis and editing; M.-D. Damaceanu: conceptualization, methodology, writing – review & editing.

Conflicts of interest

There are no conflicts to declare.

Acknowledgements

This work was supported by a grant of the Ministry of Research, Innovation and Digitization, CNCS– UEFISCDI, project number PN-III-P1-1.1-TE-2021-1110, within PNCDI III, contract no. TE 83/2022.

References

1 H. Ibrahim, A. Ilinca and J. Perron, *Renewable Sustainable Energy Rev.*, 2008, **12**, 1221–1250.
2 Y.-G. Guo, J.-S. Hu and L.-J. Wan, *Adv. Mater.*, 2008, **20**, 2878–2887.
3 J. W. Zha, M. S. Zheng, B. H. Fan and Z. M. Dang, *Nano Energy*, 2021, **89**, 106438.
4 X.-J. Liu, M.-S. Zheng, G. Chen, Z.-M. Dang and J.-W. Zha, *Energy Environ. Sci.*, 2022, **15**, 56–81.
5 H. Palneedi, M. Peddigari, G.-T. Hwang, D.-Y. Jeong and J. Ryu, *Adv. Funct. Mater.*, 2018, **28**, 1803665.
6 H. Luo, X. Zhou, C. Ellingford, Y. Zhang, S. Chen, K. Zhou, D. Zhang, C. R. Bowen and C. Wan, *Chem. Soc. Rev.*, 2019, **48**, 4424–4465.
7 Q. Zhang, X. Chen, B. Zhang, T. Zhang, W. Lu, Z. Chen, Z. Liu, S. H. Kim, B. Donovan, R. J. Warzoha, E. D. Gomez, J. Bernholc and Q. M. Zhang, *Matter*, 2021, **4**, 2448–2459.
8 Q. Li, *Nanomaterials for Sustainable Energy*, Springer, Heidelberg, 2016.
9 Q. Li, *Functional organic and hybrid nanostructured materials: Fabrication, properties, and applications*, Wiley-VCH, Weinheim, 2017.
10 B.-Y. Yu, D.-W. Yue, K.-X. Hou, L. Ju, H. Chen, C. Ding, Z.-G. Liu, Y.-Q. Dai, H. Krishna Bisoyi, Y.-S. Guan, W.-B. Lu, C.-H. Li and Q. Li, *Light: Sci. Appl.*, 2022, **11**, 307.
11 Q. Li, L. Chen, M. R. Gadinski, S. Zhang, G. Zhang, H. U. Li, E. Iagodkine, A. Haque, L.-Q. Chen, T. N. Jackson and Q. Wang, *Nature*, 2015, **523**, 576–579.
12 J. Cai, B. Xie, Y. Jiang, J. Lu, Z. Li, P. Mao, M. A. Marwat and H. Zhang, *Compos. Sci. Technol.*, 2024, **245**, 110361.
13 B. Xie, Q. Wang, Q. Zhang, Z. Liu, J. Lu, H. Zhang and S. Jiang, *ACS Appl. Mater. Interfaces*, 2021, **13**, 27382–27391.
14 B. Xie, T. Wang, J. Cai, Q. Zheng, Z. Liu, K. Guo, P. Mao, H. Zhang and S. Jiang, *Chem. Eng. J.*, 2022, **434**, 134659.
15 L. Yi, W. Huang and D. Yan, *J. Polym. Sci., Part A: Polym. Chem.*, 2017, **55**, 533–559.
16 Y. Zhuang, J. G. Seong and Y. M. Lee, *Prog. Polym. Sci.*, 2019, **92**, 35–88.
17 A. S. Hicyilmaz and A. C. Bedeloglu, *SN Appl. Sci.*, 2021, **3**, 363.
18 A. Alias, Z. Ahmad and A. B. Ismail, *Mater. Sci. Eng. B*, 2011, **176**, 799–804.
19 D. Ai, H. Li, Y. Zhou, L. Ren, Z. Han, B. Yao, W. Zhou, L. Zhao, J. Xu and Q. Wang, *Adv. Energy Mater.*, 2020, **10**, 1903881.
20 C. Qian, T. Zhu, W. Zheng, R. Bei, S. Liu, D. Yu, Z. Chi, Y. Zhang and J. Xu, *ACS Appl. Polym. Mater.*, 2019, **1**, 1263–1271.
21 B. Wan, H. Li, Y. Xiao, Z. Pan and Q. Zhang, *J. Mater. Sci. Technol.*, 2021, **74**, 1–10.
22 G. Sun, S. Zhang, Z. Yang, J. Wang, R. Chen, L. Sun, Z. Yang and S. Han, *Prog. Org. Coat.*, 2020, **143**, 105611.
23 J. W. Zha, Y. Tian, M.-S. Zheng, B. Wan, X. Yang and G. Chen, *Mater. Today Energy*, 2023, **31**, 101217.
24 R. Ma, A. F. Baldwin, C. Wang, I. Offenbach, M. Cakmak, R. Ramprasad and G. A. Sotzing, *ACS Appl. Mater. Interfaces*, 2014, **6**, 10445–10451.
25 T. Zhu, Q. Yu, W. Zheng, R. Bei, W. Wang, M. Wu, S. Liu, Z. Chi, Y. Zhang and J. Xu, *Polym. Chem.*, 2021, **12**, 2481–2489.
26 H. Tong, J. Fu, A. Ahmad, T. Fan, Y. Hou and J. Xu, *Macromol. Mater. Eng.*, 2019, 1800709.
27 X. Peng, W. Xu, L. Chen, Y. Ding, T. Xiong, S. Chen and H. Hou, *React. Funct. Polym.*, 2016, **106**, 93–98.

28 Z. Li, G. M. Treich, M. Tefferi, C. Wu, S. Nasreen, S. K. Scheirey, R. Ramprasad, G. A. Sotzing and Y. Cao, *J. Mater. Chem. A*, 2019, **7**, 15026–15030.
29 I. Butnaru, A.-P. Chiriac, C. Tugui, M. Asandulesa and M.-D. Damaceanu, *Mater. Chem. Front.*, 2021, **5**, 7558.
30 I. Bacosca, E. Hamciuc, M. Bruma and I. A. Ronova, *High Perform. Polym.*, 2010, **22**, 703–714.
31 M. Ignatova, N. Manolova, I. Rashkov, M. Sepulchre and N. Spassky, *Macromol. Chem. Phys.*, 1998, **199**, 87–96.
32 Z. P. Smith, J. E. Bachman, T. Li, B. Gludovatz, V. A. Kusuma, T. Xu, D. P. Hopkinson, R. O. Ritchie and J. R. Long, *Chem. Mater.*, 2018, **30**, 1484–1495.
33 J. Seo, W. Jang, S. Lee and H. Ha, *Polym. Degrad. Stab.*, 2008, **93**, 298–304.
34 B. B. Sauer, R. S. McLean and R. R. Thomas, *Langmuir*, 1998, **14**, 3045–3051.
35 R. Adhikari, *J. Nepal Chem. Soc.*, 2012, **29**, 96–103.
36 D. B. Haviland, C. A. van Eysden, D. Forchheimer, D. Platz, H. G. Kassa and P. Leclère, *Soft Matter*, 2016, **12**, 619–624.
37 D. Raghavan, X. Gu, T. Nguyen, M. Van Landingham and A. Karim, *Macromolecules*, 2000, **33**, 2573–2583.
38 P. Leclère, R. Lazzaroni, J. L. Bredas, J. M. Yu, P. Dubois and R. Jerome, *Langmuir*, 1996, **12**, 4317–4320.
39 R. S. McLean and B. B. Sauer, *Macromolecules*, 1997, **30**, 8314–8317.
40 T.-Y. Lo, Y.-J. Wang, D.-M. Liu and W.-T. Whang, *J. Polym. Res.*, 2015, **22**, 4.
41 E. Werner, U. Güth, B. Brockhagen, C. Döpke and A. Ehrmann, *Technologies*, 2023, **11**, 56.
42 S. N. Magonov, V. Elings and M.-H. Whangbo, *Surf. Sci.*, 1997, **375**, L385–L391.
43 M. Krea, D. Roizard and E. Favre, *Sep. Purif. Technol.*, 2016, **161**, 53–60.
44 L. Escorial, M. de la Viuda, S. Rodríguez, A. Tena, A. Marcosa, L. Palacio, P. Prádanos, A. E. Lozano and A. Hernández, *Eur. Polym. J.*, 2018, **103**, 390–399.
45 H. Chen, Y. Xiao and T.-S. Chung, *Polymer*, 2010, **51**, 4077–4086.
46 A. Tena, A. Marcos-Fernández, L. Palacio, P. Prádanos, A. E. Lozano, J. de Abajo and A. Hernández, *J. Membr. Sci.*, 2013, **434**, 26–34.
47 C. Hamciuc, G. Lisa, D. Serbezeanu, L. M. Gradinaru, M. Asandulesa, N. Tudorachi and T. Vlad-Bubulac, *Polymers*, 2022, **14**, 4715.
48 A. Tena, Á. Marcos-Fernández, M. de la Viuda, L. Palacio, P. Prádanos, Á. E. Lozano, J. de Abajo and A. Hernández, *Eur. Polym. J.*, 2015, **62**, 130–138.
49 S. Luo, K. A. Stevens, J. Park, J. D. Moon, Q. Liu, B. D. Freeman and R. Guo, *ACS Appl. Mater. Interfaces*, 2016, **8**(3), 2306–2317.
50 M. Samet, V. Levchenko, G. Boiteux, G. Seytre, A. Kallel and A. Serghei, *J. Chem. Phys.*, 2015, **142**, 194703.
51 C. Hamciuc, E. Hamciuc, T. Vlad-Bubulac, S. Vlad, M. Asandulesa and A. Wolinska-Grabczyk, *Polym. Test.*, 2016, **52**, 94–103.
52 O. Larsson, E. Said, M. Berggren and X. Crispin, *Adv. Funct. Mater.*, 2009, **19**, 3334–3341.
53 R. A. Schlitz, K. H. Yoon, L. A. Fredin, Y. G. Ha, M. A. Ratner, T. J. Marks and L. J. Lauhon, *J. Phys. Chem. Lett.*, 2010, **1**, 3292–32974.
54 H. Silau, N. B. Stabell, F. R. Petersen, M. Pham, L. Y. Yu and A. L. Skov, *Adv. Eng. Mater.*, 2018, **20**, 1800241.
55 J. S. Ho and S. G. Greenbaum, *ACS Appl. Mater. Interfaces*, 2018, **10**, 29189–29218.
56 J. Wang, Y. Long, Y. Sun, X. Zhang, H. Yang and B. Lin, *Appl. Surf. Sci.*, 2017, **426**, 437–445.

